A Shallow-Water Model for Convective Self-Aggregation

DA YANG[a,b]

[a] *University of California, Davis, Davis, California*
[b] *Lawrence Berkeley National Laboratory, Berkeley, California*

(Manuscript received 31 January 2020, in final form 6 November 2020)

ABSTRACT: Randomly distributed convective storms can self-aggregate in the absence of large-scale forcings. Here we present a 1D shallow-water model to study the convective self-aggregation. This model simulates the dynamics of the planetary boundary layer and represents convection as a triggered process. Once triggered, convection lasts for finite time and occupies finite length. We show that the model can successfully simulate self-aggregation, and that the results are robust to a wide range of parameter values. In the simulations, convection excites gravity waves. The gravity waves then form a standing wave pattern, separating the domain into convectively active and inactive regions. We analyze the available potential energy (APE) budget and show that convection generates APE, providing energy for self-aggregation. By performing dimensional analysis, we develop a scaling theory for the size of convective aggregation, which is set by the gravity wave speed, damping time scale, and number density of convective storms. This paper provides a simple modeling framework to further study convective self-aggregation.

KEYWORDS: Gravity waves; Radiative-convective equilibrium

1. Introduction

Persistent convectively coupled circulations can self-emerge over an ocean surface with uniform temperature (Held et al. 1993; Bretherton et al. 2005). These circulation patterns are sustained by significant buoyancy and pressure gradients in the planetary boundary layer (Yang 2018a,b). Intense thunderstorms are ubiquitous in the upwelling branch of the circulation; clear sky conditions prevail in the downwelling branch of the circulation. This phenomenon is known as convective self-aggregation and has been extensively simulated in computer models (Muller and Held 2012; Wing and Emanuel 2014; Holloway and Woolnough 2016; Yang 2019). Please see Wing et al. (2017) for a comprehensive review of recent studies on self-aggregation.

A suite of studies have suggested that physical processes that lead to and maintain self-aggregation are key to the development of tropical cyclones (Wing et al. 2016; Boos et al. 2016; Ramírez-Reyes and Yang 2020) and the Madden–Julian oscillation (MJO) (Yang and Ingersoll 2013, 2014; Arnold and Randall 2015; Pritchard and Yang 2016; Khairoutdinov and Emanuel 2018), which are long-term mysteries in tropical meteorology. Understanding physics of self-aggregation, therefore, would help us decipher how convection interacts with atmospheric circulations in the tropics.

Recent progress in understanding self-aggregation primarily relies on cloud-resolving models (CRMs) and general circulation models (GCMs) (Bretherton et al. 2005; Muller and Held 2012; Muller and Bony 2015; Yang 2018a, 2019, 2018b; Arnold and Putman 2018; Patrizio and Randall 2019; Wing et al. 2017). These studies have suggested that a number of physical processes can affect the development of self-aggregation, including feedbacks involving radiation, surface fluxes, water vapor, convective heating, and evaporation of rain. Studies have also suggested that, at steady state, there is a natural length scale of self-aggregation, which is of order 2000 km in the current climate (Wing and Cronin 2015; Yang 2018b; Patrizio and Randall 2019; Arnold and Putman 2018).

However, there are no simple models that can capture all basic features of self-aggregation. Some models focused on developing instability mechanisms responsible for the initial growth of aggregated circulations (Bretherton et al. 2005; Craig and Mack 2013; Emanuel et al. 2014; Beucler and Cronin 2016; Yang 2018a; Windmiller and Craig 2019), and other models focused on what maintains the circulation and sets the spatial scale at steady state (Yang 2018b; Wing et al. 2016; Arnold and Putman 2018; Patrizio and Randall 2019). There lacks a simple model that simulates the entire aggregation process, from the onset to the steady state.

Recent studies suggested that planetary boundary layer (PBL) diabatic processes are key to the development of self-aggregation (Muller and Held 2012; Naumann et al. 2017; Yang 2018a), and that horizontal buoyancy and pressure gradients in the PBL maintain the steady-state circulation (Yang 2018b; Arnold and Putman 2018; Patrizio and Randall 2019). Motivated by these studies, we present a 1D shallow-water model that simulates atmospheric flows in the PBL, roughly the lowest 2 km. With a simple convection parameterization, this model can simulate convective self-aggregation to a statistically steady state from a homogeneous initial condition. We propose that the convective heating–overturning circulation (CHOC) feedback provides energy to self-aggregated circulations, which is consistent with recent CRM results (Yang 2018a, 2019).

As a starting point, the current model focuses on reproducing the minimal simulation in Fig. 7 of Yang (2018a). In that simulation, convection self-aggregates without radiative, surface-flux, and vapor–buoyancy feedbacks, and evaporation of rain.

Corresponding author: Da Yang, dayang@ucdavis.edu

DOI: 10.1175/JAS-D-20-0031.1

Building complexity on this shallow-water model will be left for future work.

2. A boundary layer framework

We briefly review the PBL framework for self-aggregation (Naumann et al. 2017; Yang 2018a,b; Arnold and Putman 2018; Patrizio and Randall 2019). Yang (2018a) discovered that the development of convective self-aggregation is associated with increase of available potential energy (APE), which is due to the generation of APE. The generation of APE, also known as the APE production, is a process of amplifying buoyancy anomalies: heating the warm (or cooling the cold) part of the atmosphere generates APE (Vallis 2017). The APE production then requires horizontal buoyancy anomalies. In the absence of rotation, there is no force to balance horizontal buoyancy and pressure gradients in the free troposphere, so buoyancy and pressure perturbations can be effectively smoothed out by gravity waves (Charney 1963; Sobel et al. 2001; Yang and Seidel 2020; Seidel and Yang 2020). Therefore, the APE production is primarily in the PBL, which then becomes critical to the development of self-aggregation. This hypothesis was confirmed by using a vertically resolved moist static energy (MSE) analysis (Yao et al. 2020) and a suite of mechanism-denial CRM simulations (Yang 2018a).

Yang (2018b) developed a theory for what sets the horizontal scale of self-aggregation by considering dominant balances in the PBL. This theory suggests that the size of self-aggregation scales with PBL height and the square root of buoyancy variation in the PBL. This theory correctly predicts that the natural length scale of self-aggregation is of order 2000 km, and explains how the spatial scale of self-aggregation varies with climate change (see his Figs. 3 and 10). Although this theory was developed in a 2D atmosphere, it has been subsequently used to explain 3D simulation results (Arnold and Putman 2018; Patrizio and Randall 2019). This theory focused on the distance between the centers of convective regions rather than the size of the moist convection cluster, which remains as an open question.

A growing body of literature shows the importance of PBL in leading to self-aggregation (Bretherton et al. 2005; Muller and Bony 2015; Naumann et al. 2017; Colin et al. 2019) and in maintaining the steady-state circulations (Arnold and Putman 2018; Patrizio and Randall 2019). These recent studies justify the idea of constructing a shallow-water model to simulate PBL dynamics and thereby self-aggregation.

3. A shallow-water model

We construct a linear shallow-water model that simulates the dynamics of the PBL. This model only includes a minimum set of ingredients in order to reproduce the basic features of the minimal simulations presented in Yang (2018a), in which radiative, surface-flux, vapor–buoyancy feedbacks, and evaporation of rain are all absent.

In the shallow-water model, we represent the effect of convection, radiation, and surface fluxes in the continuity equation, which acts as the thermodynamic equation (Lindzen and Nigam 1987; Gill 1980). We then represent convection as a small-scale mass sink and represent the overall effect of radiation and surface fluxes as a constant and uniform mass source to the shallow-water model (no radiative and surface-flux feedbacks). In a statistically steady state, the mass sink should balance the mass source averaged over the entire domain, which can be considered as the radiative–convective equilibrium (RCE) in this shallow-water model.

There are different ways to interpret why we can represent convection as a mass sink for our shallow-water model. First, when convection occurs, there are small-scale upward mass fluxes from the PBL to the free troposphere, which is a mass sink of the PBL indeed. Second, we can view that our shallow-water model simulates the lower branch of an overturning circulation roughly with a first-baroclinic vertical structure. Then convective heating is mathematically equivalent to a mass sink to the PBL (our model) or a mass source to the upper troposphere (Matsuno 1966; Gill 1980; Lindzen and Nigam 1987; Kuang 2008; Yang and Ingersoll 2013): convective heating lowers surface pressure. The overall effect of radiation and surface fluxes does the opposite to convection, so we represent it as a mass source.

The governing equations of our shallow-water model are given by

$$\partial_t u = -\partial_x \phi - \frac{u}{\tau_d}, \tag{1}$$

$$\partial_t \phi + c^2 \partial_x u = F_c + F_l - \frac{(\phi - \overline{\phi})}{\tau_d}, \tag{2}$$

where u represents horizontal velocity ($\mathrm{m\,s^{-1}}$); ϕ represents geopotential ($\mathrm{m^2\,s^{-2}}$), and $\overline{\phi}$ represents its domain average; τ_d represents a linear damping time scale ($\mathrm{s^{-1}}$); c represents the gravity wave speed ($\mathrm{m\,s^{-1}}$); F_c represents convective heating ($\mathrm{m^2\,s^{-3}}$), which is parameterized as a mass sink, F_l represents large-scale forcings that are constant in time and space ($\mathrm{m^2\,s^{-3}}$), parameterized as a mass source. In our model, we use the mass source to represent processes that make the atmosphere more unstable; we use mass sink to represent processes that make the atmosphere more stable. The value of F_c is negative when convection is active; F_l is positive. At steady state, F_c balances F_l over the entire domain, reaching a radiative–convective equilibrium. Derivation of the linear equations is given in appendix A.

Before we provide details of the convection parameterization, we discuss a few important assumptions and simplifications. First, we assume that linear dynamics is sufficient to capture convective self-aggregation, because nonlinear contributions to the development of self-aggregation seem to be negligible in CRM simulations (see the APE analysis in Yang 2018a, 2019). Second, we assume linear damping in both u and ϕ. Although highly idealized, the linear damping seems to capture the overall damping effect at a wide range of length scales [see Fig. 10 of Kuang (2012)]. Similar to previous studies, here we use the same damping time scale for both u and ϕ for simplicity (Gill 1980; Neelin 1989). Third, we parameterize the overall effect of radiative cooling and surface fluxes as a uniform mass source F_l, mimicking the minimal simulation in Yang (2018a), in which there are no radiative and surface-flux

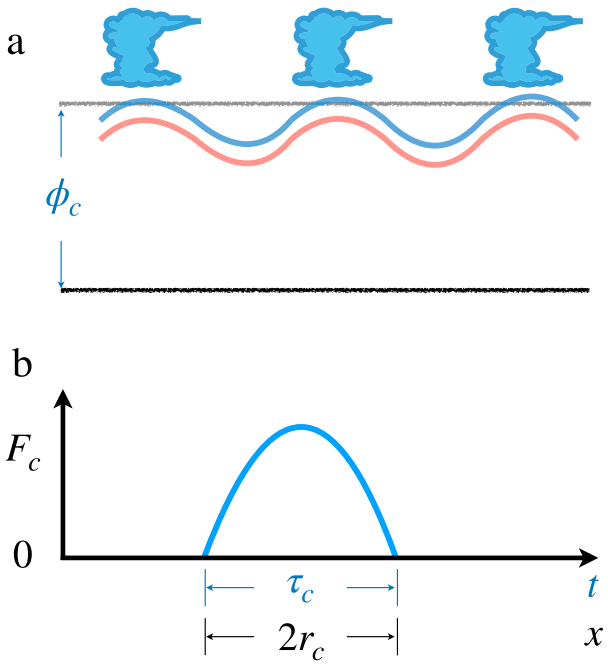

FIG. 1. Convection parameterization in the shallow-water model. (a) Anomalously high geopotential triggers convection (the blue line); anomalously low geopotential does not trigger convection (the red line). (b) Convection acts as a mass sink in our model. Each convective storm occupies length of $2r_c$ and lasts for a time period of τ_c.

feedbacks. Last, we assume that a prognostic moisture equation is not necessary. This is because the moisture–entrainment–convection feedback seems to be secondary for self-aggregation (Arnold and Putman 2018; Yang 2019).

We parameterize convection as a triggered process (Fig. 1). When ϕ exceeds a threshold ϕ_c, convection is triggered, and latent heat is released. Each convective event occupies a finite length ($2r_c$) and lasts for a finite time (τ_c):

$$F_c = -\frac{q}{r_c\tau_c}\times\left[1-\left(\frac{\Delta t-\frac{\tau_c}{2}}{\frac{\tau_c}{2}}\right)^2\right]\times\left(1-\frac{r^2}{r_c^2}\right), \qquad (3)$$

where q measures the amplitude of convection (a positive number), Δt represents the time interval since the onset of convection, and r represents the distance of a location to the convective center. F_c is zero when $\Delta t > \tau_c$ or $r > r_c$ (Fig. 1). The integrated effect of individual storms over its entire life cycle and convective area scales with q. In our model, the forcing amplitude is small, so ϕ_c is approximately equal to the equilibrium geopotential $\phi_e \equiv c^2$. This will become evident in our simulation results. Therefore, choosing a gravity wave speed also determines the triggering threshold of convection.

This convection parameterization is almost identical to that in Yang and Ingersoll (2013, 2014), who have successfully simulated the MJO in a shallow-water model. The only difference is that we parameterize the effect of convection on the PBL (the lowest 2 km), whereas Yang and Ingersoll (2013, 2014) focused on the upper troposphere. This convection scheme has been referred to as triggered convection, in contrast to quasi-equilibrium (QE) convection (Emanuel et al. 1994). Convective heating is not an instantaneous function of the thermodynamic state nor the PBL convergence. This convection scheme is, therefore, also different from the conditional instability of the second kind (CISK) (Bretherton 2003; Emanuel et al. 1994). This convection scheme proposes that convection would occur only if enough mass has been accumulated in the PBL ($\phi > \phi_c$), implying that convection lags the PBL convergence. This lag could be due to the sensitivity of deep convection to moisture and convective available potential energy (CAPE), both of which favor deep convection. For example, shallow convection gradually moistening the lower troposphere and eventually helps deep convection to develop (Hohenegger and Stevens 2013). Therefore, ϕ in our model has implicitly included information of moisture.

Here convection is triggered by *small-scale* high pressure anomalies. At first sight, this seems to be surprising because convection often occurs at low pressure areas. However, we will show that convection indeed occurs in *large-scale* low pressure environment in our shallow-water simulations (section 4). Although convection is triggered when ϕ is higher than ϕ_c, ϕ quickly falls below ϕ_c and then keeps falling until $\Delta t = \tau_c$. Therefore, convection lowers the layer thickness in an area with anomalously low ϕ during most of the convecting period. This is key to generate the large-scale low pressure environment and to simulate convective self-aggregation. We will further illustrate how convection works by using our simulation results (section 4).

In this shallow-water model, fluid dynamics is linear, and the only nonlinearity comes from the triggered convection. Therefore, the absolute amplitude of any forcing is not of interest. This is because we can scale the entire equation by any arbitrary factor, and the dynamics should remain identical. There are five free parameters: convective time scale τ_c, radius of convective storms r_c, gravity wave speed c, the damping time scale τ_d, and number density of convective events S_c. S_c is a derived parameter, measuring number of convective events per unit area per time. Over a time period T and a spatial scale L, the energy balance is given by

$$nq \sim F_l TL, \qquad (4)$$

where n represents number of convective events over T and L; S_c then emerges from this energy balance:

$$S_c \equiv \frac{n}{TL} \sim \frac{F_l}{q}. \qquad (5)$$

The integrated effect of an individual storm over its entire life cycle and convective area scales with q, which has been carefully discussed in Yang and Ingersoll (2013, 2014). We have dropped an $O(1)$ scaling factor in the above analysis, which makes the physics more transparent and does not affect the rest of the paper.

We choose a set of reference parameter values: $\tau_c = 0.6$ h, $r_c = 10$ km (the size of a storm is $2r_c = 20$ km), $S_c = 4 \times 10^{-10}\,\mathrm{m^{-1}\,s^{-1}}$ (about 276 storms per day over the 8000 km domain), $c = 20\,\mathrm{m\,s^{-1}}$, and $\tau_c = 1$ day. The parameter values are similar to those in Yang and Ingersoll (2013, 2014). To test the robustness of simulation results, we have varied all parameter values at least by a factor of 2.

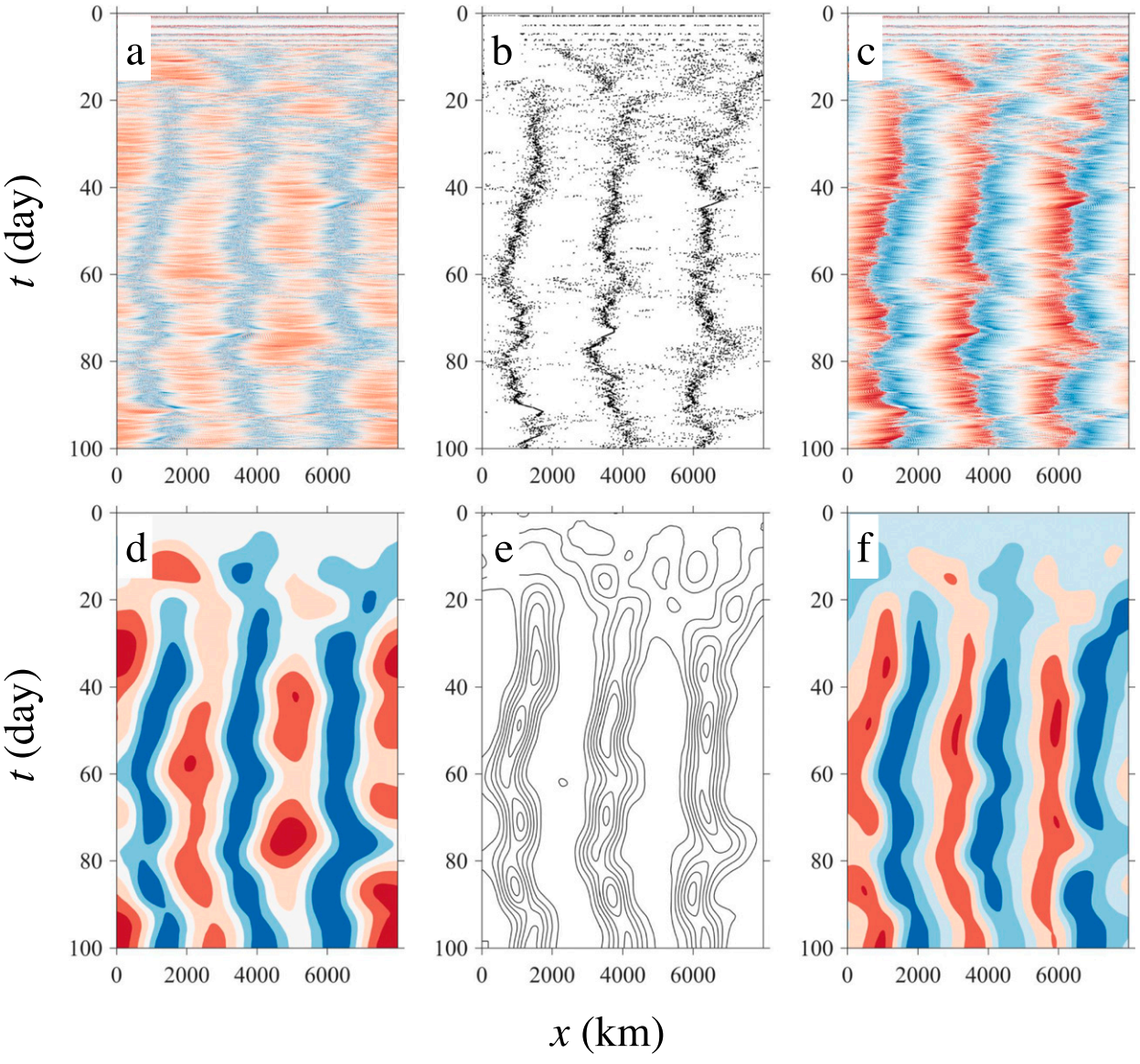

FIG. 2. A case study. (a) Geopotential anomaly from its horizontal average ϕ'. (b) Convective heating F_c. (c) Horizontal wind u. (d)–(f) The slow components corresponding to (a)–(c), respectively. The slow components are calculated as 5-day running averages of the respective fields. The forcing amplitude is arbitrarily small. Therefore, the absolute value of our model output is not important. Red represents positive, and blue represents negative. Contour and color intervals are linear.

We integrate the shallow-water model using the Lax–Wendroff method with the grid spacing $\delta x = 5$ km and time step $\delta t = 1$ min. For the reference parameter values, there are 5 grid points and 36 time steps within a convective storm, which is then well resolved. We have tested the sensitivity to δx and δt through reducing them by half, and large-scale features of the simulation results remain almost unchanged by using higher resolutions.

4. Simulation results

Our shallow-water model can successfully simulate spontaneous organization of large-scale circulations and convection. Figures 2a–c show ϕ, convection, and u of a simulation, in which $\tau_d = 0.5$ days, and all other parameters are identical to the reference parameter values. Large-scale structures in convection and circulation self-emerge quickly, reaching a statistically steady state around day 30. Convective centers collocate with large-scale low pressure centers and convergence, which is consistent with results in CRM simulations (see Fig. 2 in Yang 2018a). Within the large-scale envelopes, there are small-scale, short-lived gravity waves excited by convective storms. These gravity waves propagate toward opposite directions at the same speed, forming standing wave patterns that meander slowly. The standing wave pattern separates the domain into convectively active and inactive areas with the spatial scale of order 1000 km.

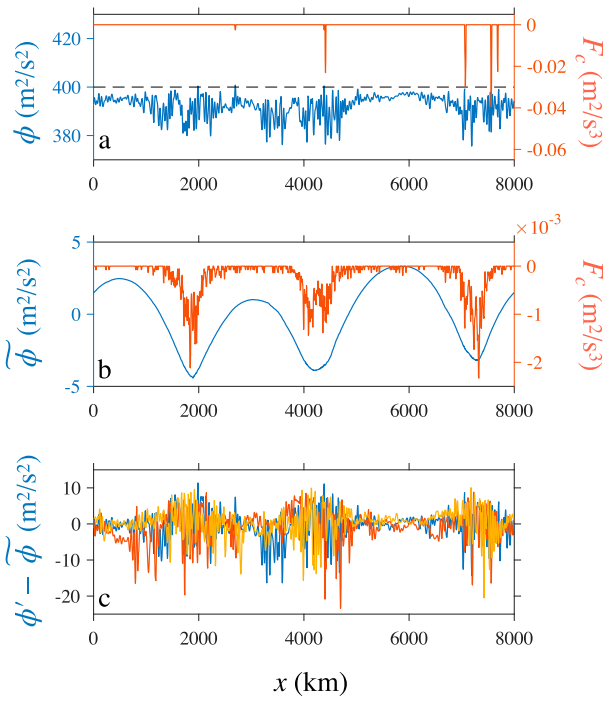

FIG. 3. The relation between ϕ and F_c at different scales. Locally, anomalously high ϕ triggers individual convective storms. However, these convective storms reside in a large-scale low pressure environment. (a) A snapshot of geopotential ϕ and convective heating F_c. The dashed line represents $\phi_c = c^2$. (b) The slow components of ϕ and F_c. They are calculated as 5-day averages. (c) Fast components of ϕ. Three snapshots with a 1-day interval. Blue shows the time shown in (a), red shows 1 day earlier, and yellow shows 1 day later.

To further illustrate how our convection scheme works, we plot a snapshot of ϕ and F_c in Fig. 3a. Convection is triggered when ϕ exceeds ϕ_c locally. This is evident, for example, at $x \approx 2500$ km and at $x \approx 4500$ km (the small orange dips). These storms span $2r_c = 20$ km in x (a much smaller scale than the convective aggregates) and will last for $\tau_c = 0.6$ hours once triggered. The amplitude of convective heating evolves with time according to (3), which is also illustrated in Fig. 1b. It will first increase and then decrease back to 0 when $\Delta t = \tau_c$. The big orange dips (e.g., at $x \approx 4500$ km and $x \approx 7000$ km) represent convective heating around the mature stage ($\Delta t = \tau_c/2$). The value of ϕ at these locations already becomes much lower than ϕ_c due to the effect of convection. Although triggered by high ϕ, convection lowers the layer thickness in an area with anomalously low ϕ during most of the convecting period.

The convective storms excite small-scale gravity waves, which then form large-scale wave envelopes (Figs. 2a,c and 3a). To better illustrate this multiscale structure, we decompose ϕ according to

$$\phi(t,x) = \overline{\phi}(t) + \phi'(t,x),\ \phi' = \tilde{\phi} + (\phi' - \tilde{\phi}), \qquad (6)$$

where $\overline{\phi}(t)$ represents domain-averaged ϕ, which is very close to c^2; ϕ' represents perturbations around $\overline{\phi}$; $\tilde{\phi}$ represents slowly varying components of geopotential anomalies (Fig. 3b, calculated as a 5-day running average); and $(\phi' - \tilde{\phi})$ represents fast components of geopotential anomalies (Fig. 3c), which are mostly gravity waves. The slow components have clear large-scale structures, corresponding to convective aggregates (Fig. 3b). The fast components have two length scales. The finescale structures are associated with individual gravity waves, and the large-scale features are wave packets—a group of gravity waves that travel together (Fig. 3c). Because these gravity waves propagate to opposite directions with the same speed, the wave packets are almost stationary in space.

These gravity waves are excited by convection, and their energy—the amplitude of waves—concentrates around convective centers (Fig. 3c), which helps trigger new convective storms nearby. This is essentially the aggregation mechanism proposed in Yang and Ingersoll (2013). The collective effect of individual storms rectifies to a large-scale mass sink, producing a large-scale low pressure environment (Fig. 3b): statistically, convection indeed resides in a large-scale low pressure environment.

We apply running average in time and space with the window widths as 5 days and 100 km, respectively. This filters out gravity waves and highlights the large-scale circulations (Figs. 2d-f). It becomes clearer that the envelope of convective heating coincides with low pressure centers throughout the entire simulation. This suggests that, at the large scale, convection generates APE, providing energy for self-aggregation.

Before we perform detailed APE analysis, we test the parameter sensitivity of our results. In each simulation, we only vary one parameter and keep the other parameters identical to those in the reference simulation (Fig. 4b). In Fig. 4, the first column presents simulations with $\tau_c = 0.4$, 0.6, and 1 h, respectively. The second column presents simulations with $r_c = 10$, 20, and 40 km, respectively. The third column presents simulations with $\tau_d = 0.5$, 1, and 2 days, respectively. The fourth column presents simulations with $S_c = 2 \times 10^{-10}$, 4×10^{-10}, and 8×10^{-10} m^{-1} s^{-1}, in which we varied F_l. The fifth column presents simulations with $c = 15$, 20, and 30 m s^{-1}. We have varied each parameter at least by a factor of 2.

Figure 4 shows horizontal wind u in a suite of simulations with a wide range of parameter values. All simulations have reproduced basic features of convective self-aggregation simulated by CRMs. Convection can self-aggregate from an initially homogeneous state, and the large-scale circulation pattern persists and reaches a (quasi-) steady state. The spatial scale of convective aggregates is about 2000–4000 km, consistent with 2D CRM results (Yang 2018b).

In all simulations, there are small-scale, short-lived gravity waves within the large-scale circulation pattern. The gravity waves propagate to both directions at $c = 15$–30 m s^{-1}, whereas the large-scale pattern remains almost in place or meanders slowly without a preferred direction. For example, in Fig. 4a, the gravity wave speed is 20 m s^{-1} (the black line). The large-scale circulation drifts to the right at about 3 m s^{-1} during the first 30 days of the simulation and then drifts to the left with the same speed for another 30 days. Such slow propagation was also observed in CRM simulations (e.g., Fig. 7 in Yang 2018a). Given that the maximum propagation speed is only about

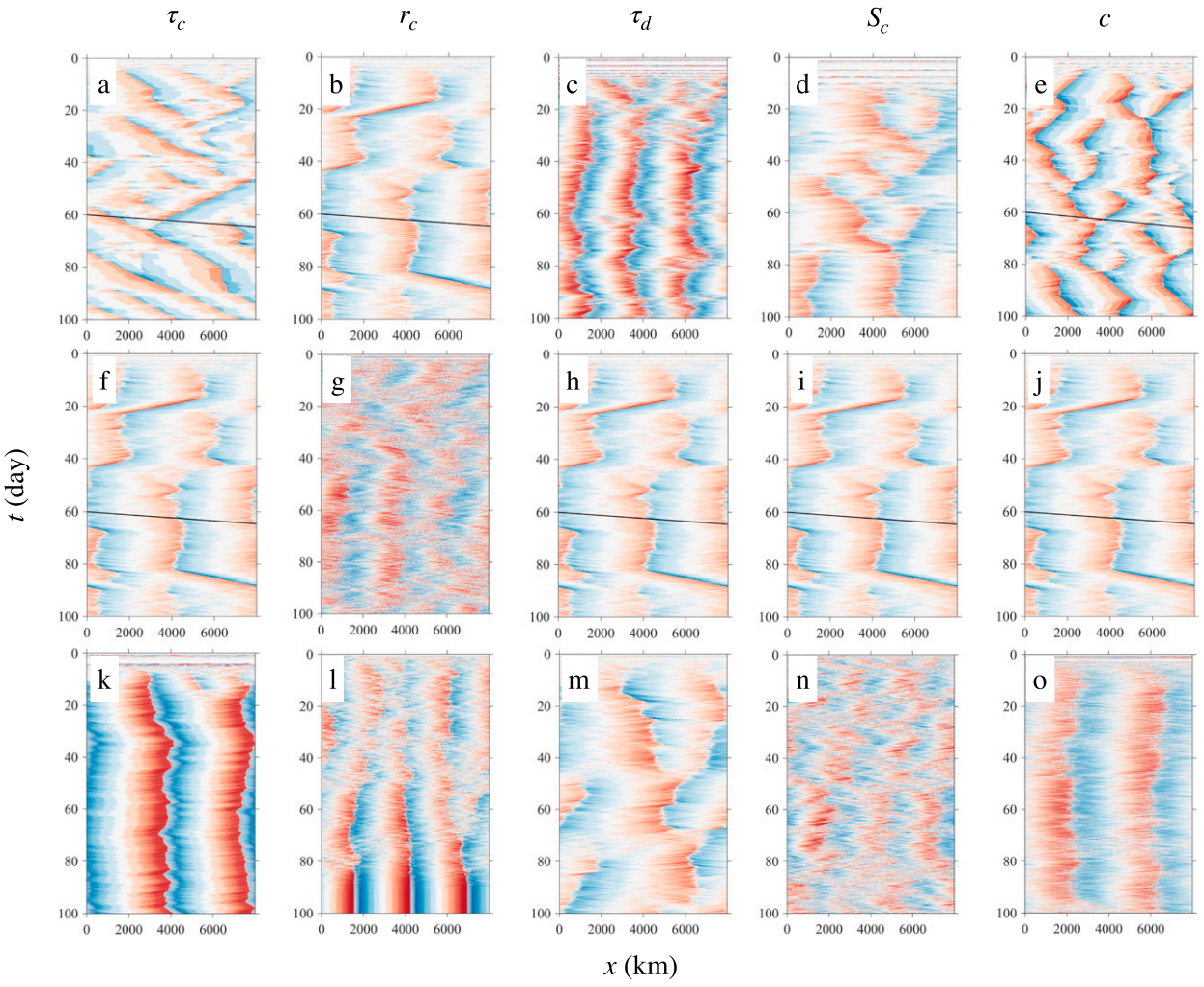

FIG. 4. Convective self-aggregation is simulated with a wide range of parameter values. Horizontal velocity u is shown in all panels. Simulations are with (a),(f),(k) $\tau_c = 0.4$, 0.6, and 1 h, respectively; (b),(g),(l) $r_c = 10$, 20, and 40 km, respectively; (c),(h),(m) $\tau_d = 0.5$, 1, and 2 days, respectively; (d),(i),(n) $S_c = 2 \times 10^{-10}$, 4×10^{-10}, and 8×10^{-10} m^{-1} s^{-1}, respectively; and (e),(j),(o) $c = 15$, 20, and 30 m s^{-1}, respectively. We have varied each parameter at least by a factor of 2. All other parameters remain the same as in the reference simulation in (b). The black lines provide the gravity wave speed in the corresponding simulations. Red represents positive, and blue represents negative. Contour and color intervals are linear.

15% of c, and that there is no preferred direction, this slow propagation is not of our interest.

In Fig. 4b, there are abrupt shifts in locations of large-scale convergence (precipitation) centers (e.g., around day 20, 40, and 80). In CRM simulations, such abrupt shifts rarely occur unless there are significant horizontal winds (e.g., Fig. B3 in Yang 2018a). This is because moisture helps localize convection: humid environment favors convection, and its associated large-scale circulations then further moisten the environment (Tompkins 2001). Here, the drift rate compares to c, and such abrupt shifts only occur in selected simulations. We have performed the APE analysis to further investigate this simulation (appendix B).

In summary, we have successfully simulated convection self-aggregation in a shallow-water model with a wide range of parameter values. The gross features of the simulated aggregates resemble those in CRM simulations, although details may differ (e.g., the abrupt shift of precipitation centers).

5. Available potential energy analysis

Now we understand what provides energy for the development and maintenance of self-aggregation at the large scale. We analyze the APE (J kg^{-1}) budget, following Yang (2018a, 2019). In the shallow-water system, we define

$$\mathrm{APE} = \frac{\overline{\phi'^2}}{2c^2}, \tag{7}$$

where $\phi' \equiv \phi - \overline{\phi}$, and $\overline{\phi}$ represents the domain average of ϕ (Gill 1982). This APE formulation corresponds well with that of a continuously stratified atmosphere [e.g., (1) in Yang 2018a]:

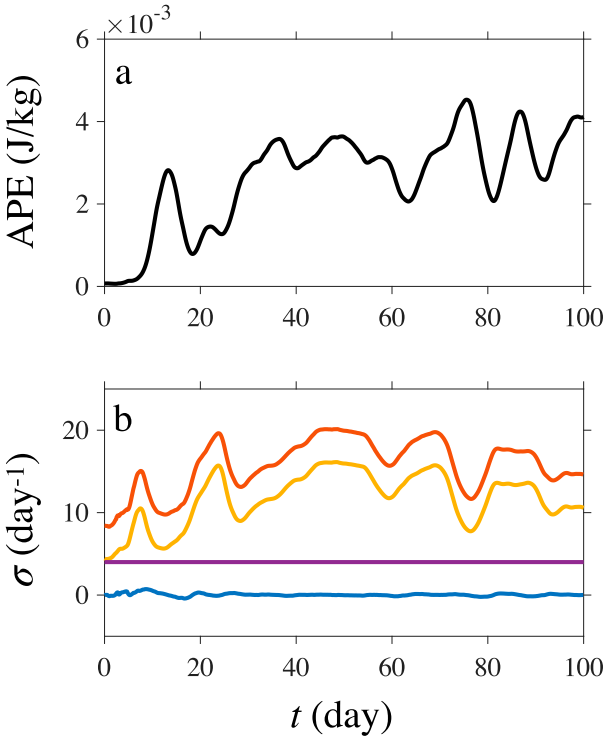

FIG. 5. The APE analysis for the simulation shown in Fig. 2. (a) Temporal evolution of APE. This is a model of linear dynamics, so the absolute magnitude of APE is not of importance. Instead, its increasing trend during the developing phase of self-aggregation is of interest. (b) APE budget. Blue represents ∂_tAPE; red represents APE production due to convective heating; yellow represents APE conversion to KE; and magenta represents sink of APE.

ϕ' is related to the buoyancy perturbation, and c^2 measures stratification.

We can derive the APE budget for convective self-aggregation, which is given by

$$\overbrace{\partial_t \frac{\widetilde{\phi}^2}{2c^2}}^{\partial_t \mathrm{APE}} + \underbrace{\overline{\widetilde{\phi}\partial_x \tilde{u}}}_{\text{Conversion to KE}} = \overbrace{\frac{\widetilde{F}_c \widetilde{\phi}}{c^2}}^{\text{APE Production}} - \underbrace{\frac{\overline{\widetilde{\phi}^2}}{c^2\tau_d}}_{\text{APE Sink}}, \tag{8}$$

where $\widetilde{(\cdot)}$ represents a slowly varying component associated with self-aggregation Yang (2018a), and $\widetilde{F}_c$ represents the slow component of anomalous convective heating.

Figure 5a shows the evolution of APE for the simulation in Fig. 2. The evolution of APE generally synchronizes with the development of convective self-aggregation. In the beginning of the simulation, APE is negligible because of the uniform initial condition. However, APE rapidly increases with time around day 7, when large-scale organization starts to appear. APE reaches a local minimum around day 20, when the aggregated circulation weakens; APE starts to grow again when the aggregated circulation strengthens. The APE oscillates around a reference value after day 40, when the aggregated circulation reaches a statistically steady state. This is in good agreement with Yang (2018a, 2019), suggesting the process of self-aggregation is associated with APE evolution.

We further show that convective heating coincides with ϕ', generating APE and providing energy for self-aggregation. Figure 5b plots

$$\sigma = \frac{\text{Eq. (8)}}{\text{APE}}, \tag{9}$$

where σ is an inverse time scale, characterizing the efficiency of generating APE due to individual processes. Larger σ indicates a shorter time scale (higher efficiency). Convective heating is most efficient in generating APE (with the largest growth rate). Once APE is generated, a large fraction quickly converts to KE, forming circulations. The sink of APE is due to the linear damping in (3): $\sigma_{\text{sink}} = 2/\tau_d = 4\,\text{day}^{-1}$. The sum of all above contributions leads to slow changes in APE with time.

Figure 5 agrees well with Figs. 3 and 4 in Yang (2018a) and Fig. 3 in Yang (2019), which show APE evolution in CRM simulations. This agreement supports that the CHOC feedback provides energy for the development of self-aggregation.

6. Spatial scale of self-aggregation

We study what sets the spatial scale of convective self-aggregation λ by using the Buckingham Π theorem. This method is based on dimensional analysis and is widely used in fluid and atmospheric dynamics (Barenblatt 2003; Yang and Ingersoll 2014; Nabizadeh et al. 2019). There are five parameters in the shallow-water model: τ_c, r_c, S_c, τ_d, and c with two dimensions—length and time. Thus, only three parameters are independent. We can choose τ_c and r_c as the reference scales to nondimensionalize the system. This choice is arbitrary and will not affect our analysis results (Barenblatt 2003).

The three free parameters define one velocity scale c and two length scales: $l_d = c \times \tau_d$, and $l_{\text{YI}} = \sqrt{c/S_c}$. Here l_d measures how far gravity waves can travel with linear damping, and l_{YI} measures how far gravity waves can travel without interfering with convective storms (Yang and Ingersoll 2014). We define the nondimensional parameters as

$$\Pi_1 = \frac{l_d}{r_c}, \quad \Pi_2 = \frac{l_{\text{YI}}}{r_c}, \quad \Pi_3 = \frac{c}{r_c/\tau_c}. \tag{10}$$

Then the length scale of self-aggregation λ is given by

$$\Pi \equiv \frac{\lambda}{r_c} \sim \Pi_1^{\alpha}\,\Pi_2^{\beta}\,\Pi_3^{\gamma}. \tag{11}$$

We can simplify (11) by focusing on intermediate asymptotics (Taylor 1950; Barenblatt 2003), in which the temporal and spatial scales of individual storms and the domain size do not affect the natural length scale of self-aggregation. This parameter regime requires

$$r_c \ll l_d, \quad l_{\text{YI}}, \quad \lambda \ll D, \tag{12}$$

and

$$\tau_c \ll \tau_d, \quad \frac{l_{\text{YI}}}{c}, \quad \frac{\lambda}{c} \ll \frac{D}{c}. \tag{13}$$

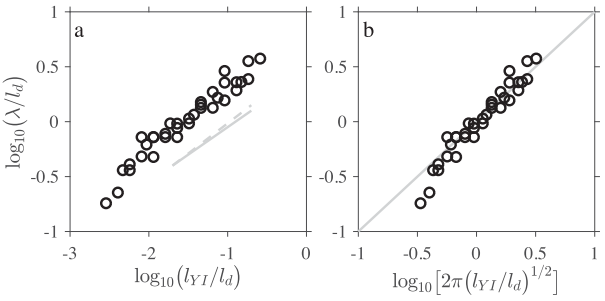

FIG. 6. Scaling analysis. (a) The log–log plot for nondimensional parameters. Each data point corresponds to one simulation. The dashed line is of 0.55 slope, which is a best fit to the data. The solid line is of 0.5 slope. (b) The log–log plot for the approximate scaling relationship. The gray line is a one-to-one line.

These are common assumptions in scaling analysis (Taylor 1950; Barenblatt 2003) and help simplify (11) to

$$\Pi \sim \Pi_1^{\alpha}\,\Pi_2^{\beta}. \tag{14}$$

By matching the dimensions on both sides of (14), we can derive $\alpha + \beta = 1$, and $\gamma = 0$. The three parameters are only constrained by two equations. Therefore, we need to perform numerical simulations to solve for α and β.

We present 20 000-km simulations with a wide range of parameter values (Fig. C1). We run each simulation for 100 days and use the last 20 days to examine the scaling relationship. We vary one parameter at a time, and both Π_1 and Π_2 are varied by over one order of magnitude. In these simulations, λ is much smaller than D for considerable parameter space, and λ increases with both l_d and $l_{\rm YI}$. Please see appendix C for more details of these large-domain simulations.

We define the size of convective aggregation as its wavelength (Yang 2018b) and diagnose λ by performing Fourier transform of u. We identify a wavenumber k that corresponds to the maximum Fourier coefficient (or spectral power) and define $\lambda = 2\pi/k$. We have also tested an alternative calculation by using a power-weighted wavenumber. The overall results remain roughly the same.

We plot the simulation results in the 10-based logarithm scale (Fig. 6a). The abscissa is $\Pi_2/\Pi_1 = l_{\rm YI}/l_d$, and the ordinate is $\Pi/\Pi_1 = \lambda/l_d$. This log–log plot shows a strong linear relationship between λ/l_d and $l_{\rm YI}/l_d$, suggesting a power-law scaling. A best-fit slope is about 0.55, and the intercept is about 0.83, approximately $\log_{10}2\pi$. This result suggests that $\alpha \approx \beta \approx 0.5$, and that the constant scaling factor is about 2π. We then propose a scaling law

$$\Pi = 2\pi\,\Pi_1^{1/2}\,\Pi_2^{1/2}, \tag{15}$$

which can be written as

$$\lambda = 2\pi(l_d\,l_{\rm YI})^{1/2}. \tag{16}$$

Figure 6b tests the scaling theory in (16). Most data points stay close to the one-to-one line, so our theory successfully explains the simulation results. Therefore, both l_d and $l_{\rm YI}$ affect the size of self-aggregation. In future studies, we would like to test (16) in CRM simulations and compare it with other theories on the spatial scale of self-aggregation (Yang 2018b; Arnold and Putman 2018).

7. Conclusions and discussion

This paper presents a shallow-water model to simulate the PBL circulation of convective self-aggregation. The simulation results resemble those of CRM simulations and are robust to a wide range of parameter values. A key component of this model is the triggered convection, which is intermittent and energetic. The convective storms interact with gravity waves, triggering new storms in the vicinity of old storms. This is a process of generating available potential energy and forming convective self-aggregation. Our results agree with Yang (2018a, 2019): the CHOC feedback provides energy for the development and maintenance of convective self-aggregation. Using dimensional analysis, we have developed a scaling theory for the size of convective aggregation. This theory succinctly fits our simulation results and suggests that two fundamental length scales l_d and $l_{\rm YI}$ together determine λ.

In the real atmosphere and comprehensive models, convection–gravity wave interactions are frequently observed: gravity waves can trigger convection, which further excites gravity waves (Fovell 2005; Uccelini 1975; Lac et al. 2002; Lane and Clark 2002; Stephan et al. 2016). We represent this interaction in our shallow-water model. Convection is triggered by anomalously high pressure in PBL (high ϕ). This situation corresponds to a cold free troposphere of reduced static stability, or equivalently a PBL with sufficiently high entropy air. Once triggered, convection will last for finite time. Convection will ventilate high entropy air in the PBL, heat the atmosphere, decrease the PBL pressure (i.e., decreasing ϕ) and excite gravity waves. This process will lead to PBL convergence, which helps accumulate high entropy air locally (i.e., increasing ϕ) and then triggers the next cycle of convection.

Adding rotation to our model recovers the Yang–Ingersoll model, which reproduces all basic features of the MJO (Yang and Ingersoll 2013, 2014). This agrees with results from convection permitting models: the MJO is a form of self-aggregation over an equatorial β plane (Arnold and Randall 2015; Pritchard and Yang 2016; Khairoutdinov and Emanuel 2018). This agreement suggests that the triggered convection scheme might have captured key aspects of how convection interacts with atmospheric flows.

This study may help explain why self-aggregation is sensitive to convection parameterizations in GCMs (Arnold and Randall 2015; Becker et al. 2017). Arnold and Randall (2015) discovered that self-aggregation emerges with explicit convection or convection parameterizations of high entrainment rates. Both scenarios depart from QE convection and allow energetic and intermittent convective storms, effectively exciting short-lived gravity waves. These gravity waves can then form standing wave patterns and separate the domain into convectively active and inactive regions. In contrast, QE convection damps small-scale, high-frequency gravity waves (Emanuel et al. 1994), so GCMs with QE

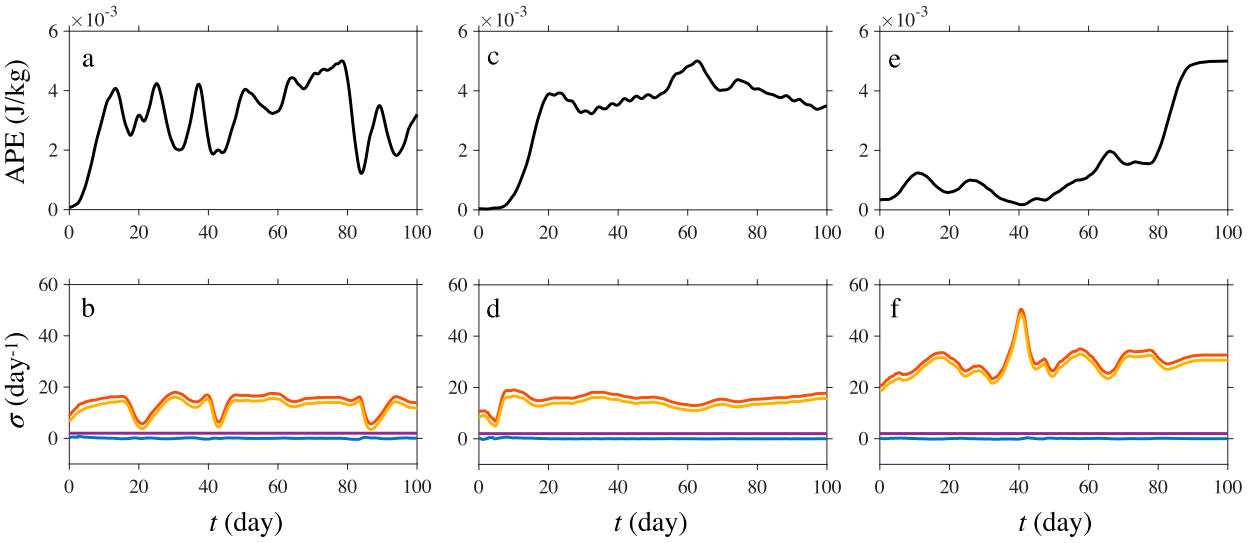

FIG. B1. APE analyses. (a),(b) Temporal evolution of APE and its budget for the simulation in Fig. 4b. (c),(d) Temporal evolution of APE and its budget for the simulation in Fig. 4k. (e),(f) Temporal evolution of APE and its budget for the simulation in Fig. 4l. Again, this is a linear model, so the absolute magnitude of APE is not of importance. Instead, its increasing trend during the developing phase of self-aggregation is of interest. Blue represents ∂_tAPE; red represents APE production due to convective heating; yellow represents APE conversion to KE; and magenta represents sink of APE.

schemes may have difficulties in simulating convective self-aggregation.

Our model is consistent with the broadly defined conditional instability of the second kind (CISK), a cooperative instability between atmospheric flows and convection that does not require radiative and surface-flux feedbacks (Bretherton 2003; Mapes 2000; Wu 2003; Kuang 2008). However, there are important differences. First, simple CISK models often parameterize convection in proportion to PBL convergence (of moisture) (Emanuel et al. 1994). In our model, however, convection requires an explicit triggering mechanism and only occurs once enough mass is accumulated in the lower troposphere, which lags the PBL convergence. This triggering mechanism could be related to the sensitivity of convection to moisture and/or convective available potential energy (CAPE). Deep convection often occurs when there is enough moisture and CAPE in the atmosphere. Second, CISK models often produce the instability at the grid scale. However, our model produces circulation patterns of thousands of kilometers, similar to those simulated in CRMs. Therefore, the CHOC feedback might be distinct from the conventional CISK (Bretherton 2003; Charney and Eliassen 1964; Lindzen 1974).

Our simple model focuses on reproducing the minimal simulation in Yang (2018a) and has inevitably omitted some physical processes that are known to be important for self-aggregation. In future studies, we would like to build up the complexity step by step to test hypotheses of convective aggregation. For example, we can add explicit moisture variables to our model to examine the sensitivity of self-aggregation to different representations of convection and associated moist processes. We can also include interactive radiation and compare the model results with other theoretical models that focus on radiative feedbacks (Bretherton et al. 2005; Emanuel et al. 2014; Beucler and Cronin 2016). Although this paper focuses on 1D simulations, we have implemented the same convection scheme to a 2D shallow-water model. The 2D model can successfully simulate convective self-aggregation, which will be presented in a future study. It is desirable to further compare our simulation results and to quantify parameter values (e.g., S_c, τ_c, and r_c) with CRM results and observations. This would advance our understanding of this triggered convection scheme and the real-world convection.

Acknowledgments. This work was supported by Laboratory Directed Research and Development (LDRD) funding from Berkeley Lab, provided by the Director, Office of Science, of the U.S. Department of Energy under Contract DE-AC02-05CH11231, and the U.S. Department of Energy, Office of Science, Office of Biological and Environmental Research, Climate and Environmental Sciences Division, Regional and Global Climate Modeling Program under Award DE-AC02-05CH11231. The author was also supported by a Packard Fellowship for Science and Engineering, and the France-Berkeley Fund.

APPENDIX A

Derivation of Linearized Shallow-Water Equations

Following Vallis (2017), nonlinear shallow-water equations are given by

$$\partial_t u + u\partial_x u = -\partial_x \phi + F_u, \tag{A1}$$

$$\partial_t \phi + u\partial_x \phi + \phi\partial_x u = F_\phi, \tag{A2}$$

where F_u and F_ϕ represent sources and/or sinks in momentum and mass, respectively. We define a constant background state

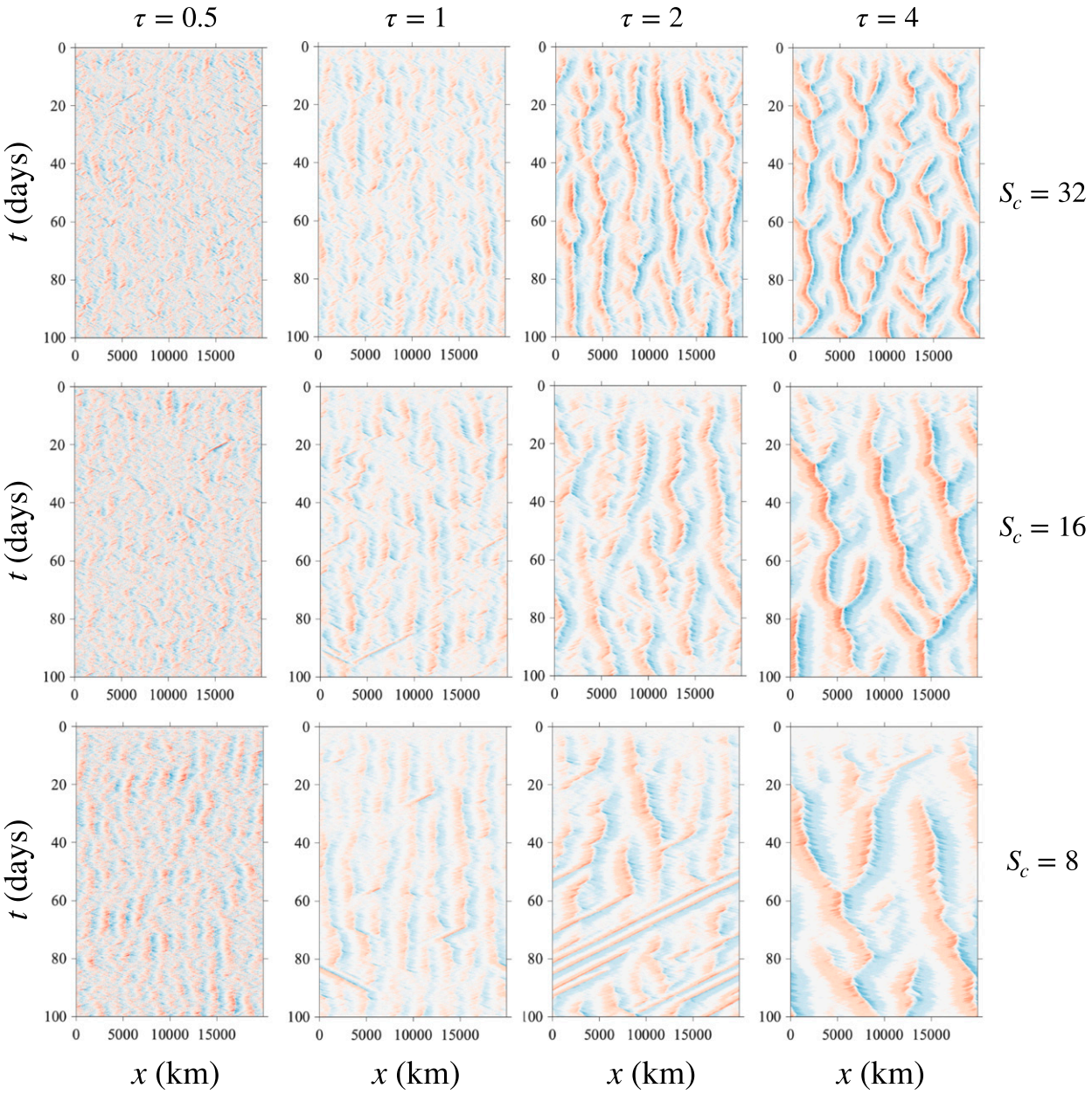

FIG. C1. Hovmöller diagram of u in the 20 000-km simulations. We have varied τ from 0.5 to 16 (days) and S_c from 2 to 32 ($\times 10^{-10}\,\mathrm{m^{-1}\,s^{-1}}$), while all other parameters remain the same as the reference parameter values. Each panel corresponds to a simulation with a specific set of parameters. Each row is with the same S_c, and each column is with the same τ. Red represents positive, and blue represents negative. Contour and color intervals are linear.

$u_0 = F_{u0} = F_{\phi 0} = 0$, and ϕ_0 and assume perturbations around the background state are small. Then we have

$$u = u_0 + \varepsilon u_1 + O(\varepsilon^2), \tag{A3}$$

$$\phi = \phi_0 + \varepsilon \phi_1 + O(\varepsilon^2), \tag{A4}$$

$$F_u = F_{u0} + \varepsilon F_{u1} + O(\varepsilon^2), \tag{A5}$$

$$F_\phi = F_{\phi 0} + \varepsilon F_\phi + O(\varepsilon^2), \tag{A6}$$

where ε is a small parameter. We substitute (A3)–(A6) to (A1) and (A2), neglect terms $O(\varepsilon^2)$, and get

$$\partial_t u_1 = -\partial_x \phi_1 + F_{u1}, \tag{A7}$$

$$\partial_t \phi_1 + \phi_0 \partial_x u_1 = F_{\phi 1}, \tag{A8}$$

where $\phi_0 = c^2$. Equations (A7) and (A8) form the set of linear shallow-water equations that are used in this paper. In the main text, we have neglected the subscript 1 for simplicity.

APPENDIX B

APE Analysis for Additional Simulations

a. Abrupt shifts in convective aggregation

We perform APE analysis to investigate the abrupt shifts in the simulation shown in Fig. 4b (e.g., around day 20, 40, and 80). Figure B1a shows that although APE quickly increases in the first 15 days, there are substantial fluctuations in APE throughout the entire simulation period. In particular, APE falls sharply around days when there are abrupt shifts. Consistently, APE production and conversion also reduces sharply around the same periods (Fig. B1b). Such reduction of APE and its production indicates tendencies of breaking up of self-aggregation. In Figs. B1c and B1d, we also show the APE analysis for the simulation in Fig. 4k, which shows no abrupt shifts. Comparing the two simulations, we find that the rapid decrease in APE and its production is likely associated with the abrupt shifts. While it is interesting to further understand this phenomenon, we will focus on convective self-aggregation for the rest of the paper and will leave the investigation of the abrupt shifts for future research.

b. Slow development of convective aggregation

We also performed the APE analysis for the simulation shown in Fig. 4l, in which we observe a slow development of self-aggregation. This is also observed in the APE evolution (Fig. B1e). This slow evolution might be related to the small *net* growth rate (longer time scales) in Fig. B1f.

APPENDIX C

Large-Domain Simulations

We present large-domain simulations of convective self-aggregation (Fig. C1). In the simulations, the domain size $D = 20\,000$ km is much larger than λ. The spatial scale of self-aggregation then would not depend on D. We vary l_d by varying τ_d from 0.5 days to 16 days; we vary l_{YI} by varying S_c from 2×10^{-10} to $32 \times 10^{-10}\,\mathrm{m^{-1}\,s^{-1}}$. We have then varied l_d and l_{YI} independently over one order of magnitude. The other parameter values are identical to those of the reference simulation. We find that the spatial scale of convective aggregates increases with both l_d and l_{YI}.

REFERENCES

Arnold, N. P., and D. A. Randall, 2015: Global-scale convective aggregation: Implications for the Madden-Julian oscillation. *J. Adv. Model. Earth Syst.*, **7**, 1499–1518, https://doi.org/10.1002/2015MS000498.

——, and W. M. Putman, 2018: Nonrotating convective self-aggregation in a limited area AGCM. *J. Adv. Model. Earth Syst.*, **10**, 1029–1046, https://doi.org/10.1002/2017MS001218.

Barenblatt, G. I., 2003: *Scaling*. Cambridge Texts in Applied Mathematics, Cambridge University Press, 171 pp., https://doi.org/10.1017/CBO9780511814921.

Becker, T., B. Stevens, and C. Hohenegger, 2017: Imprint of the convective parameterization and sea-surface temperature on large-scale convective self-aggregation. *J. Adv. Model. Earth Syst.*, **9**, 1488–1505, https://doi.org/10.1002/2016MS000865.

Beucler, T., and T. W. Cronin, 2016: Moisture-radiative cooling instability. *J. Adv. Model. Earth Syst.*, **8**, 1620–1640, https://doi.org/10.1002/2016MS000763.

Boos, W. R., A. Fedorov, and L. Muir, 2016: Convective self-aggregation and tropical cyclogenesis under the hypohydrostatic rescaling. *J. Atmos. Sci.*, **73**, 525–544, https://doi.org/10.1175/JAS-D-15-0049.1.

Bretherton, C. S., 2003: Wave-CISK. *Encyclopedia of Atmospheric Sciences*, J. R. Holton, J. A. Pyle, and J. Curry, Eds., Elsevier, 1019–1021.

——, P. N. Blossey, and M. Khairoutdinov, 2005: An energy-balance analysis of deep convective self-aggregation above uniform SST. *J. Atmos. Sci.*, **62**, 4273–4292, https://doi.org/10.1175/JAS3614.1.

Charney, J. G., 1963: A note on large-scale motions in the tropics. *J. Atmos. Sci.*, **20**, 607–609, https://doi.org/10.1175/1520-0469(1963)020<0607:ANOLSM>2.0.CO;2.

——, and A. Eliassen, 1964: On the growth of the hurricane depression. *J. Atmos. Sci.*, **21**, 68–75, https://doi.org/10.1175/1520-0469(1964)021<0068:OTGOTH>2.0.CO;2.

Colin, M., S. Sherwood, O. Geoffroy, S. Bony, and D. Fuchs, 2019: Identifying the sources of convective memory in cloud-resolving simulations. *J. Atmos. Sci.*, **76**, 947–962, https://doi.org/10.1175/JAS-D-18-0036.1.

Craig, G. C., and J. M. Mack, 2013: A coarsening model for self-organization of tropical convection. *J. Geophys. Res. Atmos.*, **118**, 8761–8769, https://doi.org/10.1002/jgrd.50674.

Emanuel, K. A., J. D. Neelin, and C. S. Bretherton, 1994: On large-scale circulations in convecting atmospheres. *Quart. J. Roy. Meteor. Soc.*, **120**, 1111–1143, https://doi.org/10.1002/qj.49712051902.

——, A. A. Wing, and E. M. Vincent, 2014: Radiative-convective instability. *J. Adv. Model. Earth Syst.*, **6**, 75–90, https://doi.org/10.1002/2013MS000270.

Fovell, R. G., 2005: Convective initiation ahead of the sea-breeze front. *Mon. Wea. Rev.*, **133**, 264–278, https://doi.org/10.1175/MWR-2852.1.

Gill, A. E., 1980: Some simple solutions for heat-induced tropical circulation. *Quart. J. Roy. Meteor. Soc.*, **106**, 447–462, https://doi.org/10.1002/qj.49710644905.

——, 1982: *Atmosphere-Ocean Dynamics*. International Geophysics Series, Vol. 30, Academic Press, 662 pp.

Held, I. M., R. S. Hemler, V. Ramaswamy, I. M. Held, R. S. Hemler, and V. Ramaswamy, 1993: Radiative–convective equilibrium with explicit two-dimensional moist convection. *J. Atmos. Sci.*, **50**, 3909–3927, https://doi.org/10.1175/1520-0469(1993)050<3909:RCEWET>2.0.CO;2.

Hohenegger, C., and B. Stevens, 2013: Preconditioning deep convection with cumulus congestus. *J. Atmos. Sci.*, **70**, 448–464 https://doi.org/10.1175/JAS-D-12-089.1.

Holloway, C. E., and S. J. Woolnough, 2016: The sensitivity of convective aggregation to diabatic processes in idealized radiative-convective equilibrium simulations. *J. Adv. Model. Earth Syst.*, **8**, 166–195, https://doi.org/10.1002/2015MS000511.

Khairoutdinov, M. F., and K. Emanuel, 2018: Intraseasonal variability in a cloud-permitting near-global equatorial aquaplanet model. *J. Atmos. Sci.*, **75**, 4337–4355, https://doi.org/10.1175/JAS-D-18-0152.1.

Kuang, Z., 2008: A moisture-stratiform instability for convectively coupled waves. *J. Atmos. Sci.*, **65**, 834–854, https://doi.org/10.1175/2007JAS2444.1.

——, 2012: Weakly forced mock Walker cells. *J. Atmos. Sci.*, **69**, 2759–2786, https://doi.org/10.1175/JAS-D-11-0307.1.

Lac, C., J.-P. Lafore, and J.-L. Redelsperger, 2002: Role of gravity waves in triggering deep convection during TOGA COARE. *J. Atmos. Sci.*, **59**, 1293–1316, https://doi.org/10.1175/1520-0469(2002)0591293:ROGWIT>2.0.CO;2.

Lane., T. P., and T. L. Clark, 2002: Gravity waves generated by the dry convective boundary layer: Two-dimensional scale selection and boundary-layer feedback. *Quart. J. Roy. Meteor. Soc.*, **128**, 1543–1570, https://doi.org/10.1002/qj.200212858308.

Lindzen, R. S., 1974: Wave-CISK in the tropics. *J. Atmos. Sci.*, **31**, 156–179, https://doi.org/10.1175/1520-0469(1974)031<0156:WCITT>2.0.CO;2.

——, and S. Nigam, 1987: On the role of sea surface temperature gradients in forcing low-level winds and convergence in the tropics. *J. Atmos. Sci.*, **44**, 2418–2436, https://doi.org/10.1175/1520-0469(1987)0442418:OTROSS>2.0.CO;2.

Mapes, B. E., 2000: Convective inhibition, subgrid-scale triggering energy, and stratiform instability in a toy tropical wave model. *J. Atmos. Sci.*, **57**, 1515–1535, https://doi.org/10.1175/1520-0469(2000)057<1515:CISSTE>2.0.CO;2.

Matsuno, T., 1966: Quasi-geostrophic motions in the equatorial area. *J. Meteor. Soc. Japan*, **44**, 25–43, https://doi.org/10.2151/jmsj1965.44.1_25.

Muller, C. J., and I. M. Held, 2012: Detailed investigation of the self-aggregation of convection in cloud-resolving simulations. *J. Atmos. Sci.*, **69**, 2551–2565, https://doi.org/10.1175/JAS-D-11-0257.1.

——, and S. Bony, 2015: What favors convective aggregation and why? *Geophys. Res. Lett.*, **42**, 5626–5634, https://doi.org/10.1002/2015GL064260.

Nabizadeh, E., P. Hassanzadeh, D. Yang, and E. A. Barnes, 2019: Size of the atmospheric blocking events: Scaling law and response to climate change. *Geophys. Res. Lett.*, **46**, 13 488–13 499, https://doi.org/10.1029/2019GL084863.

Naumann, A. K., B. Stevens, C. Hohenegger, and J. P. Mellado, 2017: A conceptual model of a shallow circulation induced by prescribed low-level radiative cooling. *J. Atmos. Sci.*, **74**, 3129–3144, https://doi.org/10.1175/JAS-D-17-0030.1.

Neelin, J. D., 1989: On the interpretation of the Gill model, *J. Atmos. Sci.*, **46**, 2466–2468, https://doi.org/10.1175/1520-0469(1989)046<C2466:OTIOTG>2.0.CO;2.

Patrizio, C. R., and D. A. Randall, 2019: Sensitivity of convective self-aggregation to domain size. *J. Adv. Model. Earth Syst.*, **11**, 1995–2019, https://doi.org/10.1029/2019MS001672.

Pritchard, M. S., and D. Yang, 2016: Response of the superparameterized Madden–Julian oscillation to extreme climate and basic state variation challenges a moisture mode view. *J. Climate*, **29**, 1995–2019, https://doi.org/10.1175/JCLI-D-15-0790.1.

Ramírez-Reyes, A., and D. Yang, 2020: Spontaneous cyclogenesis without radiative and surface-flux feedbacks. EarthArXiv, https://doi.org/10.31223/osf.io/8fshw.

Seidel, S. D., and D. Yang, 2020: The lightness of water vapor helps to stabilize tropical climate. *Sci. Adv.*, **6**, eaba1951, https://doi.org/10.1126/sciadv.aba1951.

Sobel, A. H., J. Nilsson, and L. M. Polvani, 2001: The weak temperature gradient approximation and balanced tropical moisture waves. *J. Atmos. Sci.*, **58**, 3650–3665, https://doi.org/10.1175/1520-0469(2001)058<3650:TWTGAA>2.0.CO;2.

Stephan, C., M. J. Alexander, and J. H. Richter, 2016: Characteristics of gravity waves from convection and implications for their parameterization in global circulation models. *J. Atmos. Sci.*, **73**, 2729–2742, https://doi.org/10.1175/JAS-D-15-0303.1.

Taylor, G., 1950: The formation of a blast wave by a very intense explosion. II. The atomic explosion of 1945. *Proc. Roy. Soc. London*, **201A**, 175–186, https://doi.org/10.1098/RSPA.1950.0050.

Tompkins, A. M., 2001: Organization of tropical convection in low vertical wind shears: The role of water vapor. *J. Atmos. Sci.*, **58**, 529–545, https://doi.org/10.1175/1520-0469(2001)058<0529:OOTCIL>2.0.CO;2.

Uccelini, L. W., 1975: A case study of apparent gravity wave initiation of severe convective storms. *Mon. Wea. Rev.*, **103**, 497–513, https://doi.org/10.1175/1520-0493(1975)103<0497:ACSOAG>2.0.CO;2.

Vallis, G. K., 2017: *Atmospheric and Oceanic Fluid Dynamics: Fundamentals and Large-Scale Circulation*. 2nd ed. Cambridge University Press, 860 pp., https://doi.org/10.1017/9781107588417.

Windmiller, J. M., and G. C. Craig, 2019: Universality in the spatial evolution of self-aggregation of tropical convection. *J. Atmos. Sci.*, **76**, 1677–1696, https://doi.org/10.1175/JAS-D-18-0129.1.

Wing, A. A., and K. A. Emanuel, 2014: Physical mechanisms controlling self-aggregation of convection in idealized numerical modeling simulations. *J. Adv. Model. Earth Syst.*, **6**, 59–74, https://doi.org/10.1002/2013MS000269.

——, and T. W. Cronin, 2015: Self-aggregation of convection in long channel geometry. *Quart. J. Roy. Meteor. Soc.*, **142**, 1–15, https://doi.org/10.1002/qj.2628.

——, S. J. Camargo, and A. H. Sobel, 2016: Role of radiative–convective feedbacks in spontaneous tropical cyclogenesis in idealized numerical simulations. *J. Atmos. Sci.*, **73**, 2633–2642, https://doi.org/10.1175/JAS-D-15-0380.1.

——, K. Emanuel, C. E. Holloway, and C. Muller, 2017: Convective self-aggregation in numerical simulations: A review. *Surv. Geophys.*, **38**, 1173–1197, https://doi.org/10.1007/s10712-017-9408-4.

Wu, Z., 2003: A shallow CISK, deep equilibrium mechanism for the interaction between large-scale convection and large-scale circulations in the tropics. *J. Atmos. Sci.*, **60**, 377–392, https://doi.org/10.1175/1520-0469(2003)060<0377:ASCDEM>2.0.CO;2.

Yang, D., 2018a: Boundary layer diabatic processes, the virtual effect, and convective self-aggregation. *J. Adv. Model. Earth Syst.*, **10**, 2163–2176, https://doi.org/10.1029/2017MS001261.

——, 2018b: Boundary layer height and buoyancy determine the horizontal scale of convective self-aggregation. *J. Atmos. Sci.*, **75**, 469–478, https://doi.org/10.1175/JAS-D-17-0150.1.

——, 2019: Convective heating leads to self-aggregation by generating available potential energy. *Geophys. Res. Lett.*, **46**, 10 687–10 696, https://doi.org/10.1029/2019GL083805.

——, and A. P. Ingersoll, 2013: Triggered convection, gravity waves, and the MJO: A shallow-water model. *J. Atmos. Sci.*, **70**, 2476–2486, https://doi.org/10.1175/JAS-D-12-0255.1.

——, and ——, 2014: A theory of the MJO horizontal scale. *Geophys. Res. Lett.*, **41**, 1059–1064, https://doi.org/10.1002/2013GL058542.

——, and S. D. Seidel, 2020: The incredible lightness of water vapor. *J. Climate*, **33**, 2841–2851, https://doi.org/10.1175/JCLI-D-19-0260.1.

Yao, L., D. Yang, and Z.-M. Tan, 2020: A vertically resolved MSE framework highlights the role of the boundary layer in convective self-aggregation. arXiv, https://arxiv.org/abs/2008.10158.